EUROPEAN ORGANIZATION FOR NUCLEAR RESEARCH

ALICE 2000–21
Internal Note/PHOS
4 September 2000

CHARGED PARTICLE VETO DETECTOR WITH OPEN GEOMETRY FOR THE PHOS SPECTROMETER

A.M.Blick[1)], M.Yu.Bogolyubsky[1)], A.Di Mauro[2)], S.V.Erin[1)], C.Gregory[2)], F.Hahn[2)], S.Haider[2)], M.S.Ippolitov[3)], Yu.V.Kharlov[1)], A.Klovning[4)], M.O.Lobanov[1)], O.A.Maeland[4)], P.Martinengo[2)], N.G.Minaev[1)], O.H.Odland[4)], F.Piuz[2)], R.Rongved[4)], B.Skaali[5)], S.A.Sadovsky[1)], V.D.Samoylenko[1)], I.G.Sibiriak[3)], V.I.Suzdalev[1)], V.V.Tikhonov[1)], J.Van Beelen[2)], D.Williams[2)]

1) *Institute for High Energy Physics, Protvino, Russia*

2) *CERN, Geneve, Switzerland*

3) *Kurchatov Institute of Atomic Energy, Moscow, Russia*

4) *Department of Physics, University of Bergen, Norway*

5) *Department of Physics, University of Oslo, Norway*

Abstract

The Charged Particle Veto (CPV) detector with open geometry for the photon spectrometer (PHOS) of the ALICE experiment together with beam test results of the CPV prototype in 1999 are presented.

1 Introduction

The physics motivation of the Charged Particle Veto (CPV) detector which will be installed in front of the PHOS for background suppression from charged particle hits, the relevant requirements to the CPV as well as the beam tests of the first CPV prototype were discussed in details in the PHOS TDR [1] and in our note [2]. The mentioned CPV prototype is based on proportional tubes with cathode pad read-out (pad size 22x22 mm^2). It provides different spatial resolution along ($\sigma_x = 1.25$ mm) and across ($\sigma_y = 6.4$ mm) wires.

In this Note we present the CPV prototype based on the Multi Wire Proportional Chambers (MWPC) with cathode pad read-out (so called open geometry) along with the results of beam tests of the prototype in 1999. The used gas mixture is 70 %Ag+30 %CO_2. This new CPV prototype fulfils all requirements for the CPV detector in ALICE. Particulary it provides a spatial resolution of the order of 1.5 mm along and across wires. The mentioned spatial resolution across wires is achieved due to smaller wire pitch (5.65 mm) and smaller pad size (22x10.7 mm^2) compared with the first CPV prototype.

2 Construction of the CPV Prototype

The new prototype of the CPV detector was designed and produced during summer 1999. Low-mass construction materials were used for the CPV production to minimise the material budget, radiation length and detector mass. The detector was made as a proportional chamber with a front sensitive area of 27×18 cm^2 equipped with cathode pad readout based on the GASSIPLEX chips as front-end electronics. Two cathode planes were made of 0.8 mm thick two side cooper-clad G10 foils, the outer surfaces of the cathode planes play the role of the detector electromagnetic shield. Further construction details are shown in Fig. 1.

The key element of the CPV construction is the lithographically produced pad structure on the inner copper cladding of the main cathode plane. The sensitive area consists of $18 \times 12 = 216$ pads. The pad size is 22×10.7 mm^2 elongated along wires. The pad size $a_1 = 22$ mm coincides with the transversal dimension of the PHOS scintillating crystals while the size across wires $a_2 = 10.7$ mm is practically one half of the crystal size. The gap between adjacent pads is equal to 0.6 mm.

The anode wires, made of gold-plated tungsten with 3% rhenium, are strung along the X-direction with a pitch $w = 5.65$ mm, and thus two wires cover each pad. This particularity of the CPV prototype leads to a two times better spatial resolution across the wires compared with the more common case of a single wire under each pad. The other main features of the CPV prototype are as follows:

- the anode wire diameter diameter is 30 μm,
- the anode-cathode distance is $d = 5$ mm,
- the gas mixture is 70% Ar + 30% CO_2.

3 Beam Tests

The tests of the CPV prototype were performed in August 1999 at the T10 beam line of the PS in CERN in the moment range $(1-5)$ GeV/c of different charged particles (electrons, hadrons and muons). The experimental equipment of this line included a system of trigger and Cherenkov counters as well as 4 planes of coordinate detectors based on Gas Strip Detectors (GSD) with a cathode strip read-out [3]. The aperture of the GSD was 10×10 cm^2 with strip pitch 5 mm and spatial resolution of the order of 60 μm.

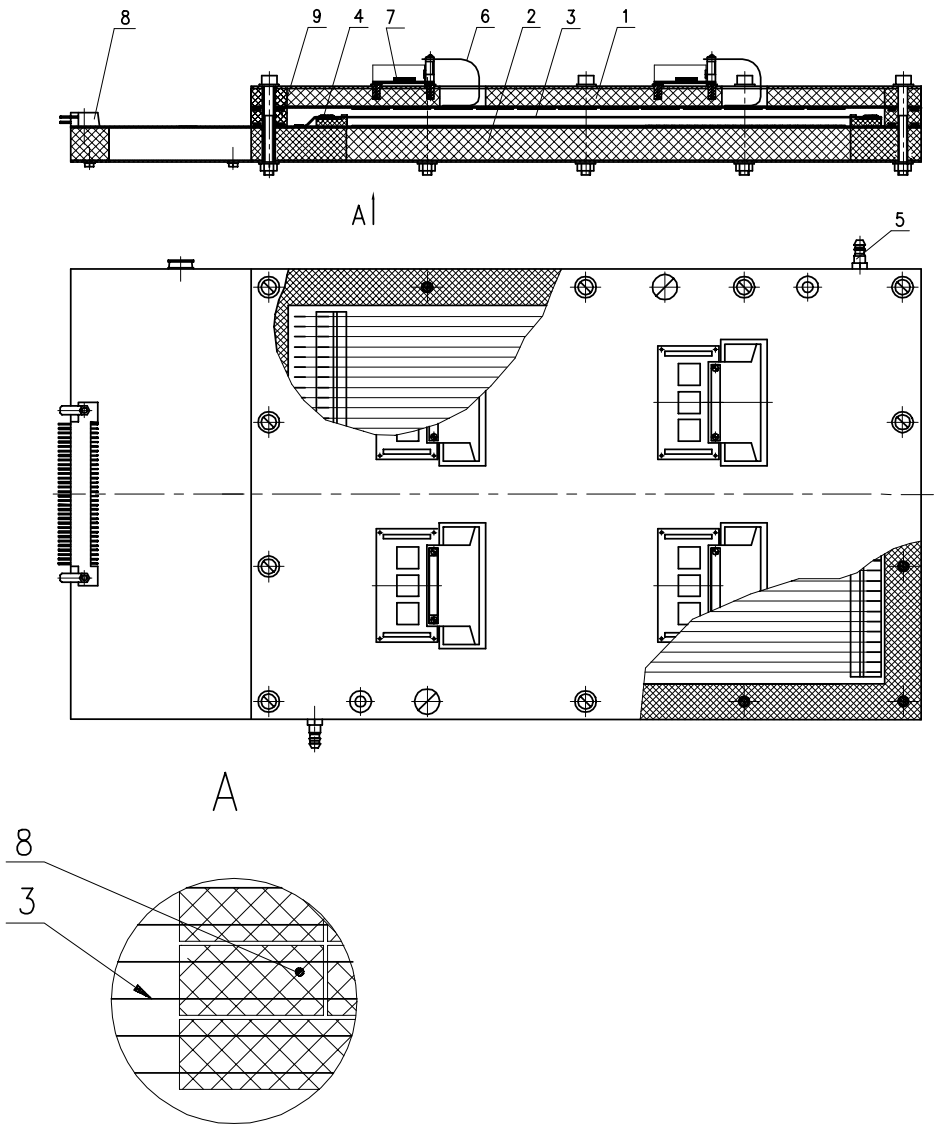

Figure 1: The CPV prototype. Notations: 1 – pad panel, 2 – cathode panel, 3 – anode wires, 4 – comb, 5 – gas inlet, 6 – cable, 7 – gassiplex, 8 – connector, 9 – frame.

For tests the CPV prototype was placed in the beam with normal orientation of its plane with respect to the beam. The anode wires were oriented horizontally, i.e. along the X-axis. The Y-axis was directed across the wires. During irradiation of the CPV prototype by charged particles the signals from cathode pads were amplified by 16-channel GASSIPLEX, transferred to 10-bit ADC's and finally stored on the DAQ computer disk. The equivalent noise charge of the GASSIPLEX-0.7-1 preamplifier with 1 μs time shaping is equal 630 e^- (r.m.s.) at 0 pF, see [9].

The front-end electronics, read-out and data acquisition were the same for the GSD and CPV. We used two standard CAEN VME modules, which served all channels of the GSD and CPV, i.e. the module V550 C-RAM [10] for analog to digital conversion and the V5551B C-RAMS Sequencer [11] for control of the signals exchange between the GASSIPLEX chips and C-RAM.

The GSD was used for beam track reconstruction. The distributions of amplitudes and cluster lengthes in the GSD are shown in Fig. 2. Further details can be found elsewhere [3]. Here we would like to point out additionally, that we selected for analysis only the events with three and more strips in the GSD clusters and with the main strip amplitude greater than 50 ADC counts.

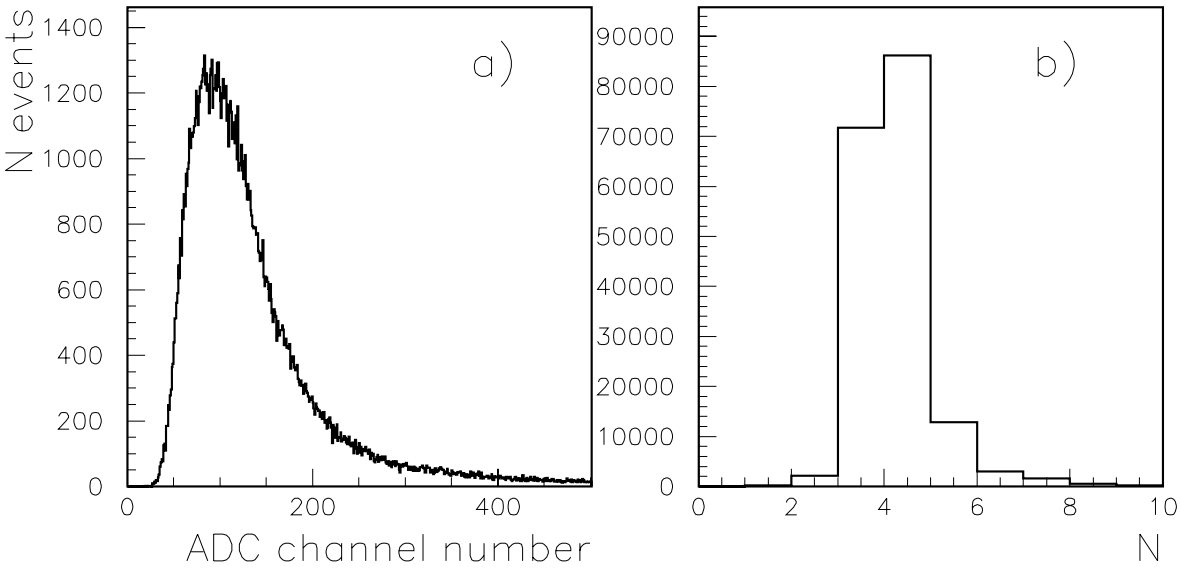

Figure 2: GSD detector: **a)** amplitude spectrum of signals for the GSD strip with the highest signal in cluster and **b)** cluster size distribution (in number of strips) **b)**.

4 Results of the CPV beam tests

4.1 Amplitude spectra and clusters

Single charged particles crossings the CPV produce clusters with dimensions N_1 and N_2 along wires (X-direction) and across wires (Y-direction) respectively. The total number of pads in the cluster $N \leq N_1 \times N_2$. The longitudinal and transverse cluster sizes in number of pads vary from one to three with negligible contribution of larger clusters. The experimental distributions of cluster sizes at high voltage 2000 V are shown in Fig.3. The cluster amplitudes essentially increase with the high voltage applied as illustrated in Fig. 4 where the high voltage dependence of the highest amplitude in clusters is shown (here and below the amplitudes are in ADC counts). As a result the relative parts of

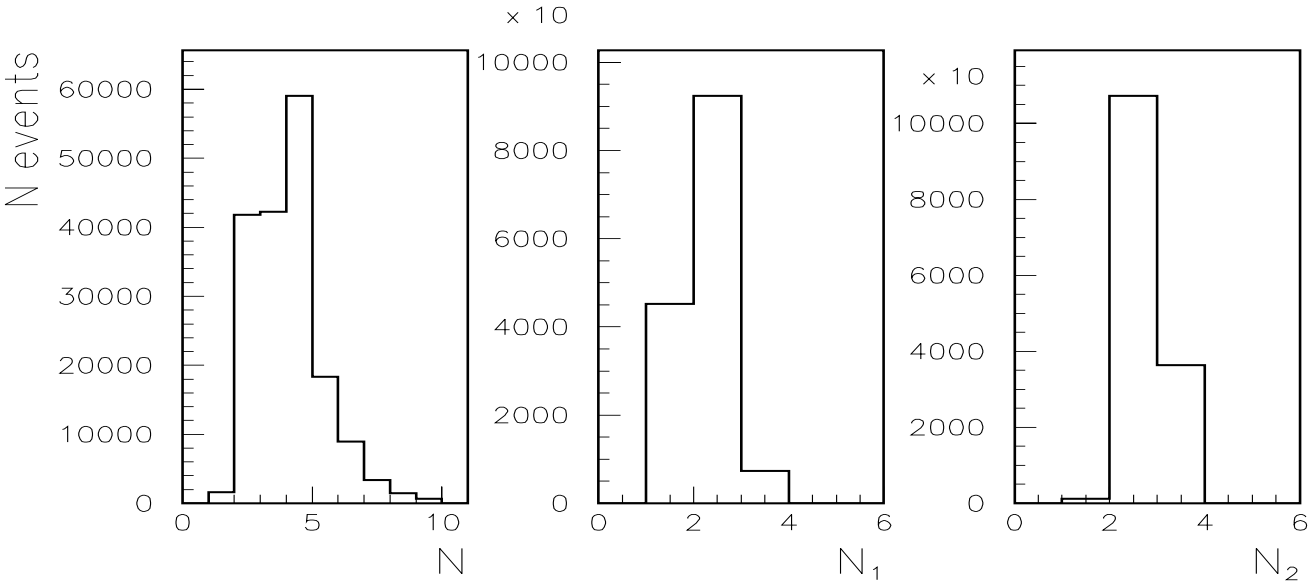

Figure 3: Experimental distributions of values N, N_1 and N_2 (all in number of pads) which are the total cluster size and cluster dimensions along and across anode wires respectively. The high voltage is 2000 V.

clusters in total sample with sizes $n = 1, 2, 3$ along X- and Y-axis, i.e. ε_{Xn} and ε_{Yn}, variate with high voltage. This dependence is shown in Fig 5. One can see that the part of clusters with sizes $n > 1$ increases with high voltage. In particular, contribution of clusters with $n = 1$ in Y-direction is less than 1% at 2000 V. In the same time 1%-contribution of clusters with $n = 1$ in X-direction can be achieved only at much higher voltage, greater than 2200 V. Fig. 6 presents the amplitude spectra at 2000 V for the pad with maximum amplitude (main pad) in cluster and two adjacent pads (relative to the main pad) in X- and Y-directions. As expected the amplitudes from Y-adjacent pads are greater than from X-adjacent pads that is explained by rectangular pad shape with larger size along wires than across ones.

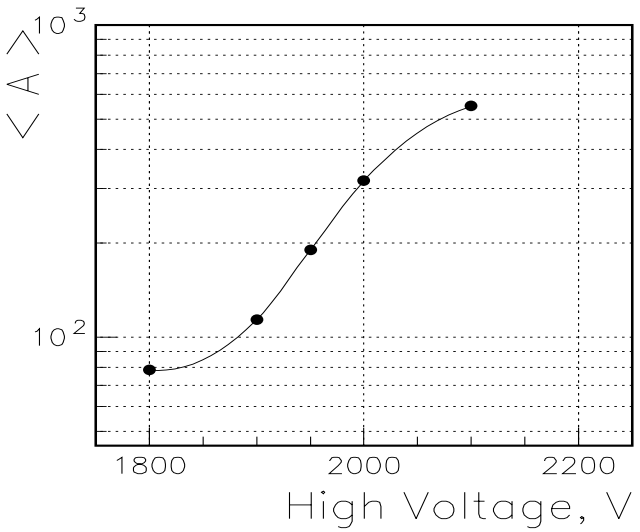

Figure 4: Increase of the average highest amplitude in clusters with high voltage growth. The solid curve represents a spline interpolation of the experimental points.

The measured amplitude spectrums, Fig. 6, are well reproduced in the framework of the CPV simulation model. This model takes into account fluctuations of energy losses on the base of Landau equation [4] with Vavilov's [5] modifications, including electrons binding energy in atoms [6] as well as gas gain statistical variations and electronics noise,

details see in papers [7, 8].

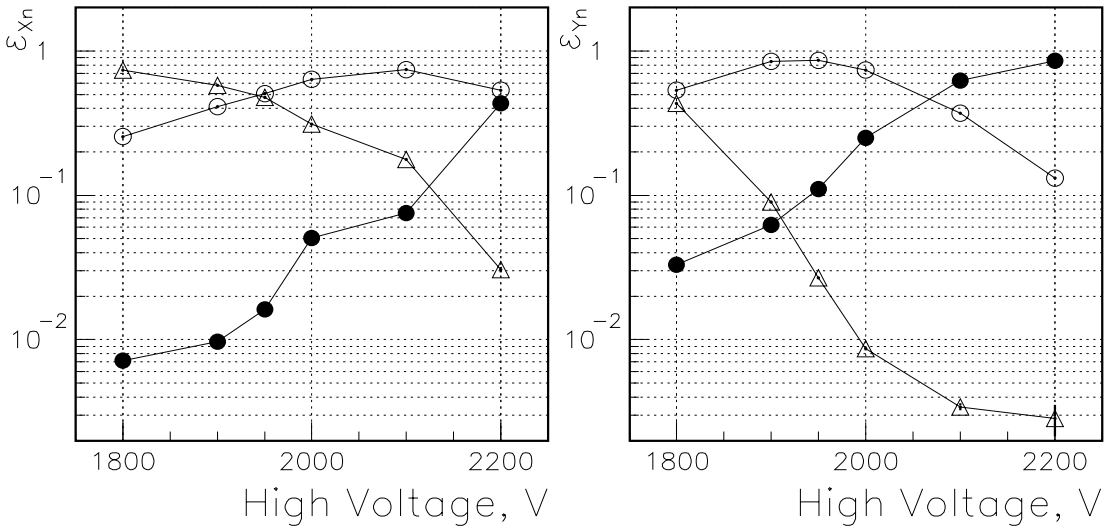

Figure 5: Contributions ε_{Xn} and ε_{Yn} of clusters with dimensions n along X- and Y-directions into the total sample as a functions of high voltage applied; here triangles, white points and black points represent data for $n = 1, 2, 3$ respectively.

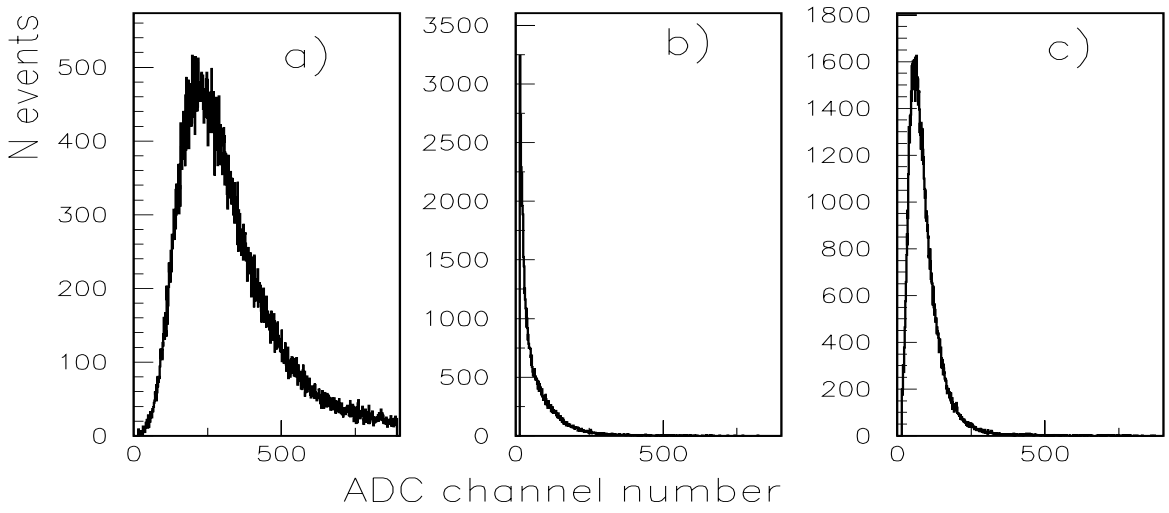

Figure 6: Amplitude spectra from the CPV cathode pads: **a)** with the maximal amplitude in the cluster (the main pad), **b)** and **c)** with the maximal amplitude from the two adjacent pads relative to the main pad in the X- and Y-directions respectively. The high voltage is 2000 V.

4.2 Detection efficiency

The detection efficiency of the CPV for charged particles was measured using the GSD detectors, the results are presented in Fig. 7 as a function of the high voltage applied. The efficiency ε demonstrates the characteristic behaviour for MWPC: it increases with growth of the high voltage up to 1900 V and then, at higher voltage values, it has an approximate plateau. On this plateau, for example at 2000 V, the efficiency is $\varepsilon \simeq 0.996 \pm 0.004$, that is quite reasonable for such kinds of detectors.

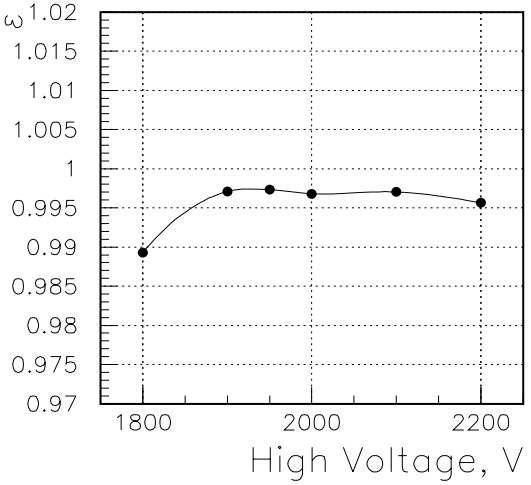

Figure 7: Charged particle detection efficiency for the CPV prototype as function of the high voltage applied. The solid curve is a spline interpolation of the experimental points.

4.3 CPV pad response function

The Pad Response Function (PRF) of the CPV relates the pad amplitudes with the position of the track avalanches relative to the pad centres. The coordinates of charged tracks were measured with high precision (60 μm) by means of 4 planes of the GSD detectors. Fig. 8 shows the average amplitudes from cluster pads as a function of the track position relative to the pad centres. This lego-plot represents the measured 2-dimensional pad response function of the CPV in terms of normalised coordinates. The normalised coordinates x', y' and variables w', a'_1, a'_2 defined as follows:

$$x' = x/d\ , \qquad y' = y/d, \qquad a'_1 = a_1/d\ , \qquad a'_2 = a_2/d, \qquad w' = w/d\ , \tag{1}$$

where d is anode-cathode distance in the CPV. The projections of this lego-plot on X- and Y-axes, that one sees in Fig. 9, give the dependences of the averaged amplitudes in

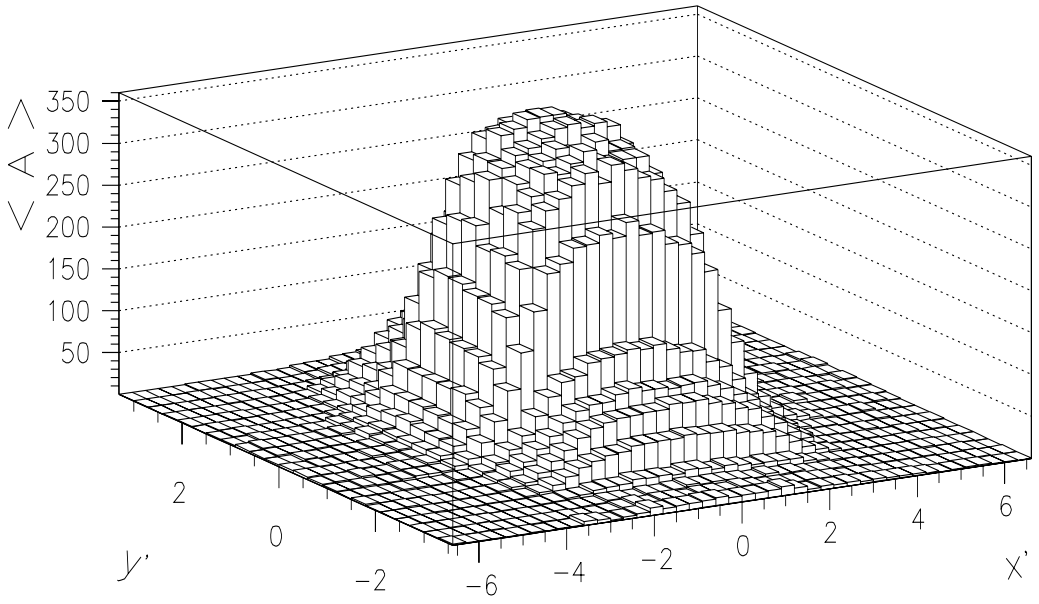

Figure 8: Lego-plot of the average amplitude detected in a pad as a function of the differences in coordinates between the hit position and the centre of the pad. The high voltage is 2000 V.

pad rows on hit coordinates counting from the row centres. These two distributions are proportional to the corresponding Strip Response Functions (SRF) $\mathbf{P_1}(x)$ and $\mathbf{P_2}(y)$.

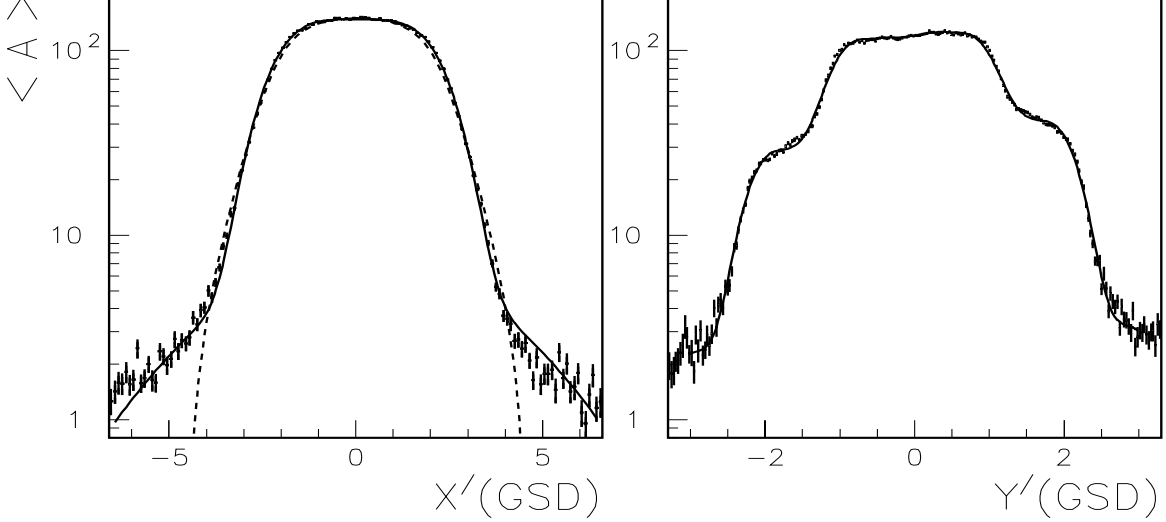

Figure 9: Dependence of the average amplitude detected in a pad on normalised x'- and y'-coordinates of hits counting from the centre of this pad. The solid lines correspond to fitted x'- and y'-approximations (4) and (8) respectively. The dashed lines show the electrostatic formula (3). The high voltage is 2000 V.

For fitting of the strip response function along X-axis we used several parameterisations: Gaussian (2), electrostatic (3) (see [8]) and sum of Gaussian and the 4-th order pseudogaussian (4):

$$f(x') = C \cdot G_2(\sigma, x') \ , \tag{2}$$

$$f(x') = \frac{C}{\pi} \cdot \sum_{i=0}^{\infty} (-1)^i \left[\arctan\left(\frac{x' + a'_1}{2i+1} \right) - \arctan\left(\frac{x' - a'_1}{2i+1} \right) \right] \ , \tag{3}$$

$$f(x') = C \cdot [G_4(\sigma, x') + \alpha_2 \ G_2(\sigma_2, x')] \ , \tag{4}$$

where we introduced notation $G_n(\sigma, x)$ for the n-th order pseudogaussian function:

$$G_n(\sigma, x) = \exp\left(-|x|^n/(n\sigma^n)\right) \ . \tag{5}$$

It sould be noted, that the 2-nd order pseudogaussian $G_2(\sigma, x)$ coincides with the common Gaussian function.

The results of the experimental data fitting are presented in Table 1. The Gaussian parameterization (2) describes well the experimental data only at $|x'/a'_1| < 0.5$, i.e. in the area of the main pad of the cluster. A good fit of the data is obtained for the paramerization coming from electrostatics (3), which contains the normalisation constant as the only one fitted parameter. This approximation fails at x'-values $|x'/a'_1| > 1$, that could be explained by an influence of electronics noise and the anode wires shielding effect, neglected in (3). An excellent fit is obtained in the full x'-interval $|x'/a'_1| < 1.5$ for paramerization with a sum of the 4-th order pseudogaussian and Gaussian (4). The obtained parameterizations of $\mathbf{P_1}(x')$ allow one to estimate the one-dimensional charge density function $\sigma_1(x')$ through the recurent relation between the $\sigma_1(x')$ and derivative $d\mathbf{P_1}/dx'$ of the strip response function, details see elsewhere [8]. In our case, taking into account the boundary condition $\sigma_1(-\infty) = 0$, this relation has the form:

$$\sigma_1(x') = \frac{d\mathbf{P_1}(z = -x' + a'_1/2)}{dz} + \sigma_1(x' - a'_1) \ . \tag{6}$$

The obtained charge density function is shown in Fig.10. Calculations were performed on the base of parameterization (4) of the strip response function. Here, for comparison,

Table 1: Fitted parameters for average amplitudes (after projection on X- and Y-axis) as different functions of x'- and y'- coordinates relative to the strip centres. The references to the amplitude equations are shown in the column labelled as Eq, the fit intervals are given in terms of the corresponding pad size as $|x'/a_1'| < m$ for x'-approximations (2), (3), (4) and as $|y'/a_2'| < m$ for y'-approximation (8).

Eq.	m	C	σ	σ_2	α_1	α_2	α_3	α_{-1}	α_{-2}	α_{-3}	$\frac{\chi^2}{N_p}$
(2)	0.5	155.2 $\pm$1.5	2.23 $\pm$0.04								$\frac{35}{46}$
(3)	1.	322.6 $\pm$2.1									$\frac{36}{92}$
(4)	1.5	139.6 $\pm$1.3	1.814 $\pm$.011	3.18 $\pm$.19		0.056 $\pm$.008					$\frac{93}{138}$
(8)	1.5	115.2 $\pm$1.2	0.435 $\pm$.003		0.394 $\pm$.005	0.131 $\pm$.002	0.010 $\pm$.001	0.365 $\pm$.004	0.092 $\pm$.002	0.008 $\pm$.001	$\frac{51}{201}$

we show also the theoretical prediction for the same charge density function obtained in electrostatics, see [8].

$$\sigma_1^{theor}(x') = \frac{C}{\pi} \cdot \sum_{i=0}^{\infty} (-1)^i \ \frac{2i+1}{x'^{\,2} + (2i+1)^2} \ , \tag{7}$$

where C is the normalisation constant that can be found from the condition:

$$\int_{-\infty}^{\infty} \sigma_1^{theor}(x') d\, x' = 1 \ .$$

The experimental curve is normalised to the theoretical one in the point $x' = 0$.

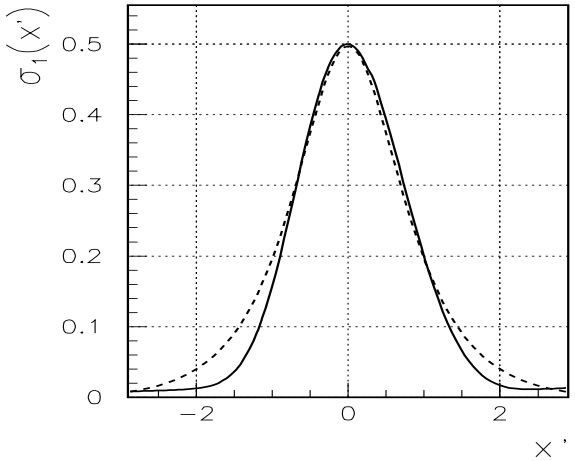

Figure 10: Experimental one-dimensional charge density function $\sigma_1(x')$ (solid curve) and theoretical prediction of this function (dashed curve) in electrostatics (7). The experimental curve is normalised to the theoretical one at point $x' = 0$. The high voltage is 2000 V.

As for the SRF function across the wires $\mathbf{P_2}(y)$ the experimental data demonstrates bright structures corresponding to the contribution of six anode wires, see Fig.9, which affect the cluster pads in the case of our CPV geometry. The data were successfully fitted with a sum of six pseudogaussians of the 3-rd order, which corresponds up to six active wires in clusters:

$$f(y') = C \cdot \sum_{i=1}^{3} \left[\alpha_i \ G_3 \left(\sigma, y' - w'(i - 1/2) \right) + \alpha_{-i} \ G_3 \left(\sigma, y' + w'(i - 1/2) \right) \right] \tag{8}$$

with an additional normalisation condition for the fitted parameters

$$\sum_{i=1}^{3}(\alpha_i + \alpha_{-i}) = 1. \tag{9}$$

The shifts $\pm w'(i-1/2)$ of arguments in (8) correspond to the positions of wires relative to the centre of the main pad in cluster. The obtained values of parameters are presented in Table 1 and shown also in Fig.11 as a function of i. One can see that the main contribution comes from the two central wires.

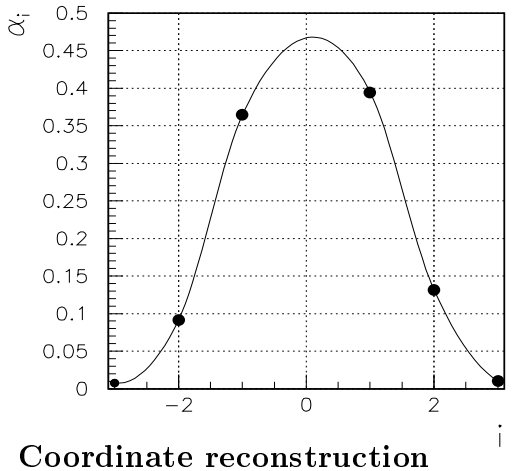

Figure 11: Dependence of the coefficients α_i on i. The solid lines present a spline interpolation of the experimental results. The high voltage is 2000 V.

5 Coordinate reconstruction

The methods of coordinate reconstruction for detectors with strip and pad readout are discussed in details in paper [8]. Here we point out only the main steps of the procedure. At the first step of coordinate reconstruction in the CPV one searches clusters among the CPV amplitudes above some threshold. The found 2-dimensional clusters gives pairs of 1-dimensional clusters after projection on the X- and Y-axes. The analysis of the projected clusters reduces the 2-dimensional problem of coordinates determination in the CPV to a 1-dimensional problem like in the case of strip read-out.

Below we assume that channels in 1-dimension clusters are ordered by index i in such manner, that the index value $i = 0$ relates to the channel with the maximal signal in the cluster (main strip). The negative and positive values of i give adjacent left and right side strips respectively.

5.1 One-point formula

For one-strip clusters the optimal estimation of the hit coordinate is determined by the strip centre x_0. The spatial resolution in this case depends on the effective size $\tilde{a}$ of the region occupied by 1-strip clusters. If a charged particle crosses a strip far away from its centre (i.e. closer to the strip edge), then as a rule, it generates a two-strip cluster. The relative contribution of 1-strip clusters ε_1 in the total sample is equals to the value $\tilde{a}/a$, where a denotes the strip width. As a result one can estimate the spatial resolution for the one-point formula as

$$\sigma_x \simeq \varepsilon_1 \cdot a/\sqrt{12}\ .$$

5.2 Two-point formula

For calculation of the hit coordinate along wires in the case of 2-strip cluster we used an empirical formula suggested in ALICE Note [2]

$$x = \pm a \cdot \alpha \cdot \frac{\ln(A_{\pm 1}) - \ln(A_0)}{\ln(A_{\pm 1}) + \ln(A_0)}\ , \tag{10}$$

where x is the hit coordinate counted from the boundary between adjacent strips in the cluster and α is an empirical constant. We have found that $\alpha = 1$ for the present CPV prototype.

5.3 Three-point formula

For calculation of coordinates along wires in the case of 3-strip clusters we used the formula from paper [12] obtained in assumption about gaussian shape of the strip response function:

$$x = -\frac{a}{2} \cdot \frac{\ln(A_1) - \ln(A_{-1})}{\ln(A_1/A_0) + \ln(A_{-1}/A_0)} \ , \tag{11}$$

where x is the hit coordinate counted from centre of the main strip in cluster.

5.4 Centre-of-gravity formula

The common centre-of-gravity formula we use for estimation of the hit coordinate across wires:

$$x = \frac{\sum_i A_i \cdot x_i}{\sum_i A_i} \ . \tag{12}$$

To diminish the effect of a systematic shift with this formula we perform beforehand the amplitudes redefinition in accordance with the original paper [3] as follows

$$A_i \to A_i - b \sum_j A_j \ , \tag{13}$$

where A_i is the amplitude of the i-th channel, parameter $b = 0.015$ and index j runs over all cluster strips. Formula (12) is applied then for redefined strip amplitudes with rejection of channels with zero or negative values of the redefined amplitudes.

5.5 N-point formula, $N \geq 3$

For calculation of coordinates in the case of N-strip clusters, $N \geq 3$, (mainly for the GSD detector) we used the formula suggested in paper [8], which obtained in assumption about gaussian shape of the strip response function

$$x = -\frac{a}{2} \cdot \frac{< i \cdot \ln(A_i/A_0) > \cdot < i^4 > - < i^2 \cdot \ln(A_i/A_0) > \cdot < i^3 >}{< i^2 \cdot \ln(A_i/A_0) > \cdot < i^2 > - < i \cdot \ln(A_i/A_0) > \cdot < i^3 >} \ , \tag{14}$$

where x is the hit coordinate relative to the centre of main strip in cluster. The other notations are as follows

$$< i^k > = \sum_i i^k \cdot W_i \ , \ k = 2, 3, 4, \tag{15}$$

$$< i^k \cdot \ln(A_i/A_0) > = \sum_i i^k \ln(A_i/A_0) \cdot W_i \ , \ k = 1, 2 \tag{16}$$

and the weight of the i-th point W_i is defined as

$$W_i = \left[\ (A_0^{-2} + A_i^{-2} \ ) \cdot (\sigma_{noise}^2 + \sigma_{digit}^2) \ \right]^{-1} \ , \tag{17}$$

where σ_{noise} is an electronic noise in numbers of ADC counts, σ_{digit} is the distortion due to digitization of amplitudes and pedestals

$$\sigma_{digit} = \sqrt{2/12} \ .$$

It should be mentioned also that formula (14) was used for data treatment after the amplitude redefinition (13) in accordance with paper [3].

5.6 Coordinates correction

The above mentioned formulae in all cases give rather good estimations of charge particle coordinates. Nevertheless the accuracy of these formulae can be improved if one introduces small additional corrections to the obtained coordinates. The reason for this is that in a real experiment there are some deviations of the used parameterizations from experimental data. We found that it is sufficient to make linear corrections of coordinates with two parameters β and γ:

$$x \to x + (\beta x + \gamma) \ . \tag{18}$$

6 CPV Spatial Resolution

In the case of 1-strip clusters the estimated value of coordinates x and y are defined by the position of the strip centre. In the case of two- and three-strip clusters the x-coordinates are calculated by formulae (10) or (11) with subsequent linear corrections (18). The y-coordinates are reconstructed by the centre-of-gravity method (12) with further linear corrections. The correction of y-coordinate is defined only by the parameter $|\gamma| = w/2$ (18), where w is the wires pitch, the coefficient $\beta = 0$. The correction sign is defined by the sign of difference $A_1 - A_{-1}$ for lateral strip amplitudes. The explanation of this correction is coming from two wires under CPV pads.

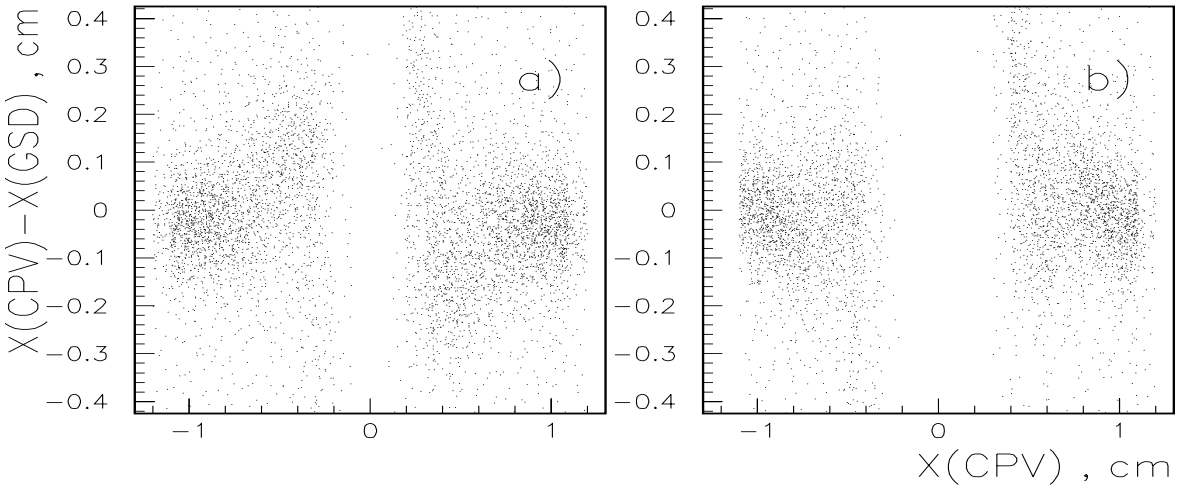

Figure 12: Two dimensional plot of the measured difference $X(CPV) - X(GSD)$ vs $X(CPV)$ for 2-strip clusters without correction **a)** and with linear correction **b)**. High voltage is 2000 V.

For x-coordinates the additional correction is smaller than for y-cordinates. The essential corrrection is obtained only for 2-strip clusters. In Fig. 12 we present the scatter plot of the differences Δx between the CPV and GSD coordinates vs the measured CPV x-coordinates for 2-strip clusters without linear correction and with it.

The white vertical gap in Fig. 12 passing through the centre of pad is explained by the contribution from 1- and 3-strip clusters, while 2-strip clusters occupy the edges of pads. Fig. 13 shows the scatter plots of the corrected X- and Y-coordinates measured in the CPV vs the same coordinates measured in the GSD-detector.

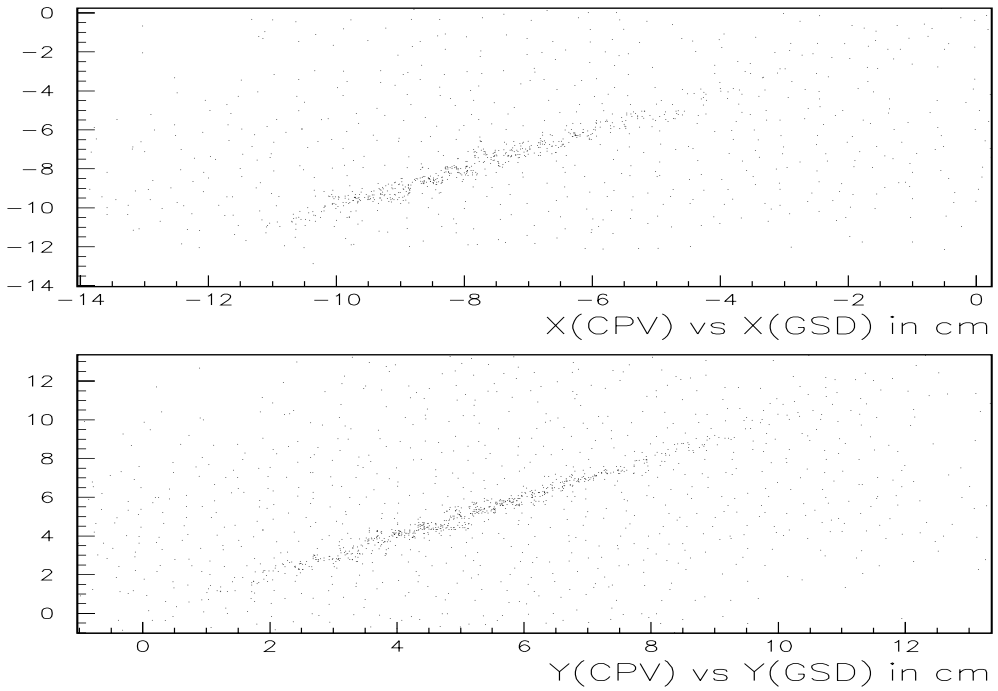

Figure 13: Correlations between corrected X- and Y-coordinates in the CPV- and in the GSD-detectors. The high voltage is 2000 V.

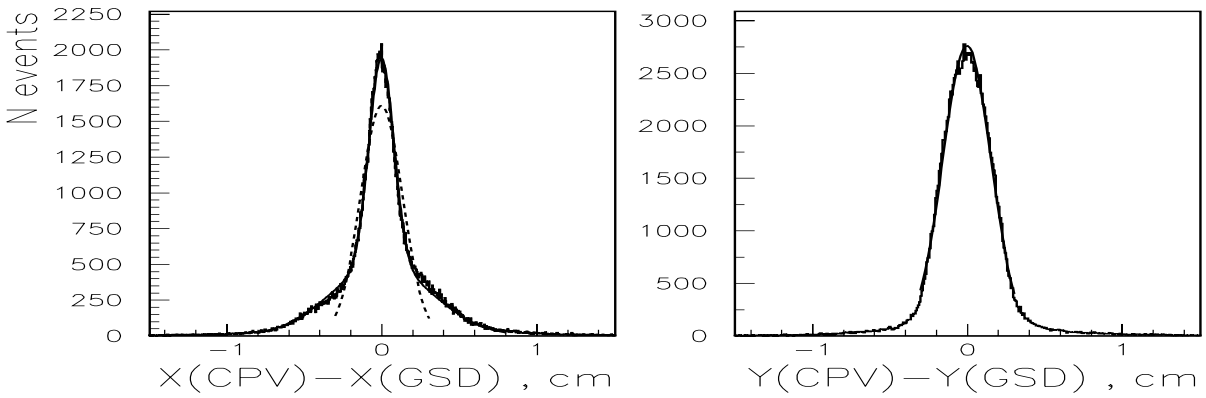

Figure 14: Difference of X- and Y-coordinates measured with the CPV- and GSD- detectors together with results of the fit. The solid lines shows a double Gaussian fit (19) for the x-coordinate and a single Gaussian fit for the y-coordinate respectively. The dashed line shows a single Gaussian fit for the x-coordinate. The obtained values of spatial resolution are $\sigma_x = 0.138 \pm 0.001$ cm and $\sigma_y = 0.154 \pm 0.001$ cm. The high voltage is 2000 V.

Fig. 14 shows the differences Δx and Δy of X- and Y-coordinates measured by CPV and GSD detectors together with the results of the experimental data fitting by Gaussian in intervals $|\Delta x| < 0.4$ cm and $|\Delta y| < 0.9$ cm. The obtained resolutions are as follows: $\sigma_x = (0.135 \pm 0.001)$ cm and $\sigma_y = (0.154 \pm 0.001)$ cm.

Nevertheless, as one sees from Fig. 14 the Δx-distribution is not fitted sufficiently well with a single Gaussian only that can be explained by the essential contribution of 1-strip clusters. A better fit in wide interval $|\Delta x| < 0.9$ cm can be performed by the sum of two Gaussians

$$f(\Delta x) = C \cdot [\ \alpha_1 \cdot G_2(\sigma_1, \Delta x) + (1 - \alpha_1) \cdot G_2(\sigma_{23}, \Delta x)\ ]\ , \qquad (19)$$

where α_1 is the relative contribution of 1-strip clusters in the total sample, σ_{23} and σ_1 are spatial resolutions for 2-3 strip clusters and 1-strip clusters respectively. The effective spatial resolution σ_x can be estimated then through the relation

$$\sigma_x^2 = \frac{\sigma_1^2 \cdot N_1 + \sigma_{23}^2 \cdot N_{23}}{N_1 + N_{23}} \ , \tag{20}$$

where N_1 and N_{23} are the numbers of events collected by relevant Gaussians in equation (19). The results are presented in Table 3. The obtained value $\sigma_x = (0.138 \pm 0.001)$ cm is in good agreement with the first estimation shown in Tab. 2.

Table 2: Spatial resolution σ_x and σ_y (in cm) as a function of the projected cluster size n in number of strips.

	$n = 1$	$n = 2$	$n = 3$	all
σ_x	0.317 ± 0.002	0.103 ± 0.001	0.121 ± 0.001	0.135 ± 0.001
σ_y	0.204 ± 0.002	0.148 ± 0.001	0.152 ± 0.001	0.154 ± 0.001

Table 3: Fitting parameters of the x-coordinate differences, measured in the CPV and GSD detectors in interval $|\Delta x| < 0.9$ cm for all clusters with size from one to three, by function (19). The value σ_x is calculated according to formula (20).

α_1	σ_1, cm	σ_{23}, cm	σ_x, cm
0.254 ± 0.002	0.310 ± 0.002	0.0799 ± 0.0012	0.138 ± 0.001

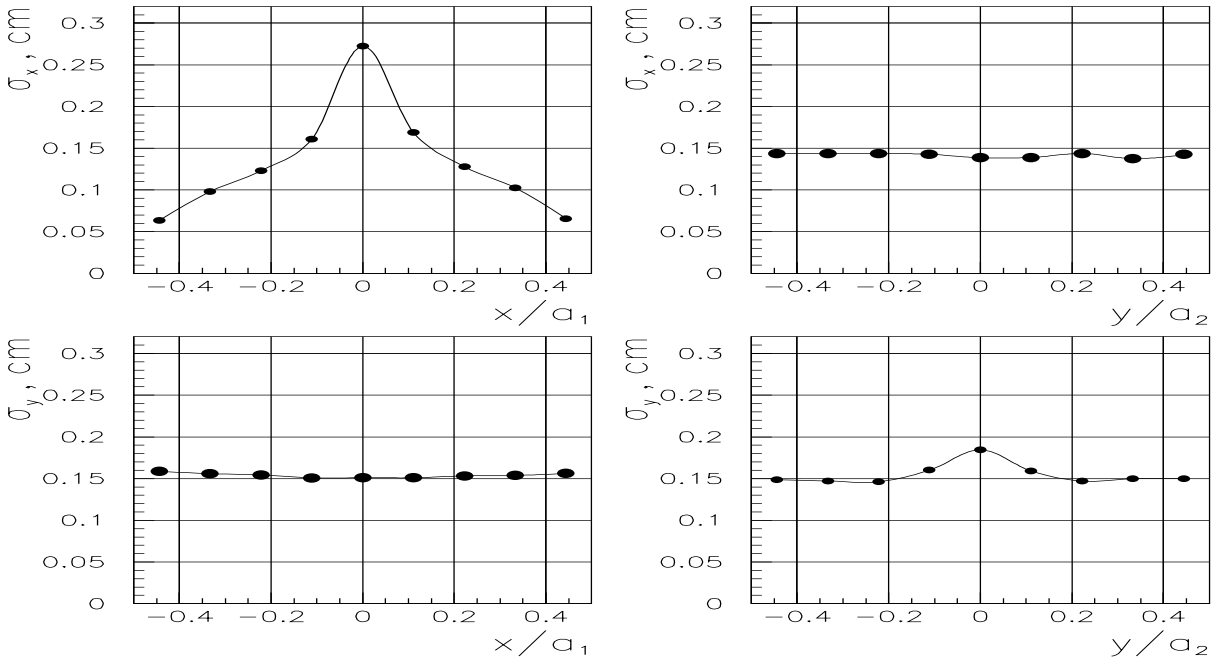

Figure 15: Dependence of the CPV spatial resolution σ_x and σ_y on the normalized x'- and y'-coordinates of hits defined relative to the centre of the main pad in a cluster. The solid lines are spline interpolation of the experimental points. The high voltage is 2000 V.

Table 4: Albedo effect: ratio N/N_0 as a function of the distance L between the CPV and the lead brick at energies of beam particles (electrons) 2 GeV and 4 GeV, where N is the number pad in detected clusters and N_0 is the same value and at the same conditions but without the lead brick.

Energy, GeV	L, cm	N/N_0
2 GeV	0.	1.054 ± 0.003
	1.5	1.050 ± 0.003
	3.	1.015 ± 0.003
	5.	1.010 ± 0.003
	8.	$1. \pm 0.003$
	10.	$1. \pm 0.003$
4 GeV	0.	1.087 ± 0.003
	1.5	1.067 ± 0.003
	3.	1.062 ± 0.003
	5.	1.041 ± 0.003
	8.	1.036 ± 0.003
	10.	1.028 ± 0.003

The spatial resolution varies with a cluster size. This is seen from Table 2 where the data are presented separately for 1-strip, 2-strip and 3-strip clusters. The best result is achieved for 2-strip clusters. Fig. 15 shows dependence of the CPV spatial resolutions σ_x and σ_y on x- and y-coordinates of hits defined relatively to the strip centre.

For σ_x the worst spatial resolution is observed in the centre of strip, it improves closer to the strip edge. The smooth initial growth of the σ_x with increase of the hit point distance from the pad edge is property of the 2-point formula (see our paper [8]), but central bump is explained by the essential contribution of 1-point clusters. Actually there is no variation of the σ_x with changing of the y- coordinate. Similar conclusion is valid for σ_y, but dependence of the σ_y is observed on the y-coordinate with minor bump in the centre of pad due to smaller contribution of 1-point clusters. There is no essential variation of the σ_y with changing of the x-coordinate.

7 Albedo effect

To simulate the PHOS influence on the CPV performance, i.e. the albedo effect for the CPV, we fulfilled a number of measurements in electron beam at energies $2 - 4$ GeV with an additional lead brick installed at different distances (variated from zero to ten cm) behind the CPV detector. The width of brick along the beam was 10 cm (≈ 18 radiation lengthes), i.e. close to the longitudinal size of PHOS crystals (20 X_0). The main results coming from these measurements are as follows: we saw a slight increase of the average number of pads in detected clusters, as it is presented in Table 4, but a degradation of the CPV spatial resolution practically was not observed.

8 Conclusions

We have presented the prototype of Charged Particle Veto detector for the PHOS spectrometer based on multiwire proportional chambers with cathode pad readout. The rectangular pads have sizes 2.2×1.07 cm^2. The results of prototype beam tests showed that the spatial resolutions along and across wires are equal to $\sigma_x \simeq 0.14$ cm and $\sigma_y \simeq 0.15$ cm

respectively. The charged particle detection efficiency is $\varepsilon \simeq 0.996$. Taking into account the small material budget, the absence of hydrogen in the operating gas mixture and low neutron sensitivity we conclude: the tested CPV prototype fulfils all requirements for the CPV detector in ALICE.

The authors would like to thank W.Klempt, V.I.Manko, V.F.Obraztsov, N.E.Tyurin for support of this work.

References

[1] ALICE Collaboration, Photon Spectrometer PHOS, Technical Design Report. ALICE TDR 2, CERN/LHCC 99-4, 5 March 1999.

[2] A.M.Blick, M.Yu.Bogolyubsky, A.Di Mauro at al., Internal Note ALICE/PHOS 99-08, 28 February 1999.

[3] F.Piuz, R.Roosen and J.Timmermans, Nucl. Instrum. and Meth. 196 (1982) 451-462.

[4] L.D.Landau, J.Phys, USSR, **8**, 201 (1944) (see also in russian: L.D. Landau, Collections of papers, V. 1, p. 482, Nauka, Moscow, 1969).

[5] P.V.Vavilov, Sov. Phys. -JETP **5**, 749 (1957).

[6] O.Blunck and S.Leisegang, Z.Phys **128**, 500 (1950);
U.Fano, Rev. Nucl. Sci. **13**, 201 (1963);
H. Bichsel and P.Saxon, Phys. Rev. **A11**, 1286 (1975).

[7] A.M.Blick et al., Charged Particle Detector Based on Proportional Tubes with Cathode Pad Readout,Preprint IHEP, Protvino, 2000 (to be published).

[8] M.Yu.Bogolyubsky et al, Coordinate Reconstruction in Gaseous Detectors with Cathode Strip and Pad Readout, Preprint IHEP, Protvino, 2000 (to be published).

[9] ALICE Collaboration, High Momentum PID TDR, ALICE TDR 1, CERN/LHCC 98-19, 1998.

[10] C.A.E.N., Technical Information Manual, mod. V550, 2-channel C-RAMS, 9 April 1998.

[11] C.A.E.N., Technical Information Manual, mod. V551B, C-RAMS SEQUENCER, 9 July 1999.

[12] I.Enddo, T.Kawamoto, Y.Mizuno et al., Nuclear Instruments and Methods 188 (1981) 51-58.